Journal of Sound and Vibration (2000) **233**(3), 515–543
doi:10.1006/jsvi.2000.2838, available online at http://www.idealibrary.com on IDEAL®

NUMERICAL ANALYSIS OF ROTATIONALLY SYMMETRIC SHELLS BY THE MODAL SUPERPOSITION METHOD

T. A. Smith

U.S. Army Aviation and Missile Command, Redstone Arsenal, AL 35898, *U.S.A.*

(*Received* 7 *May* 1999, *and in final form* 13 *December* 1999)

The system of differential equations governing the analysis of rotationally symmetric shells under time-dependent or static surface loadings is formulated with the transverse, meridional, and circumferential displacements as the dependent variables. The thickness of the shell may vary, and four homogeneous boundary conditions may be prescribed at each boundary edge of the shell. The governing differential equations for each Fourier harmonic are obtained by use of Fourier series in the circumferential direction of the shell. Influence coefficients at each of the node points along the shell meridian are obtained for each Fourier component by employing ordinary finite difference representations for the meridional co-ordinate derivatives. With these influence coefficients, a set of homogeneous flexibility equations governing the free vibration characteristics of the shell is obtained and solved for the frequencies and mode shapes for each Fourier component. The solutions under time-dependent or static surface loadings and due to initial displacements and velocities are then obtained by expanding the solutions in terms of the modes of free vibration of the shell for each Fourier component. The solution for the total shell response is obtained by Fourier series summation. Solutions for typical shells have been found to be in excellent agreement with solutions by the method of temporal and spatial finite differences. Solutions for a parabolic shell are presented as an example. The solution is also presented for a published cylindrical shell example and is seen to be in excellent agreement with the published finite element method results.

1. INTRODUCTION

In the absence of closed-form solutions for the general shell problem, several investigators have obtained solutions by numerical methods. These investigators include Penny [1], who solved the symmetric bending problem of a general shell in 1961 by finite differences; Radkowski, *et al.* [2], who solved the axisymmetric static problem in 1962 by finite differences; and Budiansky and Radkowski [3], who employed finite difference methods to solve the unsymmetrical static bending problem in 1963.

The solution to the static problem of rotationally symmetric shells of revolution subjected to both symmetrical and non-symmetrical loading was obtained also by Kalnins [4] in 1964. Starting with the equations of the linear classical bending theory of shells, in which the thermal effects were included, Kalnins derived a system of eight first order ordinary differential equations which he solved by direct numerical integration over preselected segments of the shell. Gaussian elimination was used to solve the resulting system of matrix equations obtained by providing continuity of the fundamental variables at the segmental division points.

In 1965, Percy *et al.* [5] also developed a finite element technique for the analysis of shells of revolution under both axisymmetric and asymmetric static loading by idealizing the shell as a series of conical frusta.

0022-460X/00/230515 + 29 $35.00/0

The solution for the free vibration characteristics of rotationally symmetric shells with meridional variations in the shell parameters by means of his multi-segment direct numerical integration approach was also obtained by Kalnins [6] in 1964. Subsequently, in 1965, the solution for the response of an arbitrary shell subjected to time-dependent surface loadings was obtained by Kraus and Kalnins [7] by means of the classical method of spectral representation. The solution was expanded in terms of the modes of free vibration as determined previously by Kalnins [6], and the orthogonality of the normal modes was proved for an arbitrary shell.

In 1966, Klein [8] also published an article in which he describes a matrix displacement finite element approach to the linear elastic analysis of multi-layer shells of revolution under axisymmetric and asymmetric dynamic and impulsive loadings. The method of solution involves the idealization of the shell as a series of conical frusta joined at nodal circles.

Subsequently, Smith [9, 10] published reports containing numerical procedures for the analysis of rotationally symmetric thin shells of revolution under time-dependent impulsive and thermal loadings. The field equations consisted of eight first order partial differential equations with respect to the meridional co-ordinate of the shell, and the solution for each Fourier harmonic was obtained by employing low order finite difference representations for all time and spatial derivatives.

In 1973, Smith [11] published a report giving numerical procedures for finding the dynamic response of rotationally symmetric thin shells of revolution under time-dependent surface and thermal loadings utilizing a higher order finite difference representation of spatial derivatives than that used in references [9] and [10]. The field equations consisted of eight first order differential equations, while the time derivatives were represented by ordinary backward finite differences, thus resulting in stable implicit solutions for all choices of the time increment.

In 1973, Bushnell [12] compared the finite difference energy method and the finite element method for stress, buckling, and vibration analysis of shells of revolution. In reference [12], several finite element and "finite difference element" models are discussed. Bushnell [13] uses model 4 described therein, in which the tangential displacements u_i and v_i are staggered between the normal displacements w_{i-1} and w_i. This results in a "finite difference element" which is incompatible in normal displacements and derivatives thereof at element boundaries. It is also stated in reference [12] that for "finite difference element" model 6, for which the displacements u_i, v_i, and w_i are established at the same set of points and the integration areas for membrane and bending energy are the same, numerical results were unsuccessful and that discontinuities may exist for all variables at element boundaries. It is also indicated in reference [12] that for "finite difference element" model 7, for which the displacements u_i, v_i, and w_i are taken at the same set of points but by use of different integration areas for membrane and bending energies, successful numerical results were found in a limited number of cases. We thus observe that numerical difficulties are associated with the formulations of references [12, 13] for both the case of a finite difference mesh with the displacements u_i and v_i staggered with respect to the displacements w_i and for the case for which u_i, v_i and w_i are taken at the same set of points in the finite difference mesh.

In 1975, Radwan and Genin [14] published their development of the equations for the determination of the non-linear response of thin elastic shells of arbitrary geometry under either static or dynamic loading through the use of assumed, known, or calculated mode shape functions. The geometric non-linearities were considered by employing the strain–displacement relations of the Sanders–Koiter non-linear shell theory. Introduction of the mode shape functions into the system of governing equations leads to a system of ordinary differential equations for the generalized time co-ordinates.

In 1975 also, Bathe *et al.* [15] published their reviews and development of a general finite element incremental formulation for the non-linear static and dynamic analysis of systems with large displacements, large strains, and material non-linearities. Numerical solution of the continuum mechanics equations was achieved by use of isoparametric finite element discretization. Solutions involving large displacements and large strains were presented. Numerical time integration of the finite element equations of motion is used for dynamic analysis. Inasmuch as the given development is general, it is naturally applicable to the finite element analysis of shell structures by use of successive time steps in the case of dynamic analysis.

In 1977, Smith [16, 17] published reports giving numerical procedures for the analysis of rotationally symmetric thin shells of revolution under continuous time-dependent distributed surface and thermal loadings by formulation of the system of equations in terms of the transverse, meridional, and circumferential displacements of the shell as the dependent variables and use of both a high order finite difference representation of the spatial derivatives and explicit relations for the dependent variables for the second and succeeding time increments.

In 1983, Chang *et al.* [18] published their development of procedures for the linear dynamic analysis of rotationally symmetric shells using finite elements and modal expansion. This involved the use of doubly curved axisymmetric shell finite elements in conjunction with Fourier series expansions for the loadings and dependent variables in the circumferential direction of the shell.

In 1983, Smith [19, 20] presented numerical formulations for determining both static and dynamic solutions for rotationally symmetric thin shells of revolution subjected to distributed loadings which may be discontinuous. Formulation of the system of equations was in terms of the three displacements as the dependent variables and use of an ordinary finite central difference representation for the spatial derivatives..

In 1985, Kwok [21] published an excellent description of his use and the advantages of the curvilinear finite difference (CFD) energy method for the geometrically non-linear static analysis of general thin shells of arbitrary geometry, pointing out therein that no limitations to applying it to the solution of shell structures involving material non-linearities, temperature-dependent materials, and dynamic loadings should be expected. Kwok adopted the Newton–Raphson iterative method to solve his equations in lieu of a linear incremental approach.

In 1988, Naraikin [22] published his development of a method for the dynamic analysis of shells by which the field equations were represented by a system of eight linear first order partial differential equations with four displacements and four forces as the dependent variables. Solutions are indicated for only homogeneous boundary conditions; and the displacements, internal forces, and loads are represented in the circumferential direction of the shell by Fourier series expansions. Fourier transformations in the time variable produce a system of equations which is integrated numerically to obtain fundamental solutions which are subsequently converted to the time domain by an inverse Fourier transformation.

In 1989, Teng and Rotter [23] published their development of a new doubly curved isoparametric finite element formulation for the elastic–plastic large deflection analysis of shells of revolution under axisymmetric and torsional static loading. Although only these loadings were considered in reference [23], the development used a Fourier series representation of the displacement variables in the circumferential direction of the shell and was presented in a manner to facilitate extension to non-symmetric bifurcation buckling from the primary axisymmetric path and to elastic non-symmetric non-linear analysis.

In 1988, Wimmer [24] published his application of a two-dimensional Hermitian finite difference method to the static analysis of thin plates and arbitrarily curved shells of

laminated construction for which a linear shear deformation theory was used. The basic system of equations was formulated in tensor notation as a system of first order equations which is transformed to algebraic form by use of appropriate two-dimensional Hermitian finite difference operators. Since the system of equations is given in tensor notation, shells of arbitrary curvature may be analyzed under static application of loads.

In 1991, Smith [25] completed development of procedures for determining the total shell response of any rotationally symmetric general shell under time-dependent (or static) surface loadings by the modal superposition method. The solutions treated there are accomplished by first determining the free vibration characteristics of the shell through the use of influence coefficients for the discretized shell. Subsequently, the time-dependent solution is expanded in terms of the modes of free vibration of the shell to obtain the total shell response as a summation of the several modal contributions. The procedures used are analogous to those given by Norris *et al.* [26] and illustrated therein by a simply supported beam.

In 1991, Moy and Lam [27] reported their formulations for both a ring element and a quadrilateral shell finite element for the geometrically non-linear analysis of either thin or thick axisymmetric shells under static loadings. The development is based upon the use of internal transverse shear stress unknowns to alleviate the problem of shear locking associated with thin shell finite element formulations. Good agreement between the buckling loads found by use of these new elements and published earlier results were indicated in the report.

In 1994, Smith [28] published a second report in which numerical procedures were demonstrated for determining the dynamic response of rotationally symmetric open-ended thin shells of revolution under continuous time-dependent distributed surface and thermal loadings by use of a high order finite difference representation of the spatial derivatives and explicit expressions for the displacement variables within the boundary edges of the shell for the second and succeeding time increments. Reference [28] constitutes a revision to the formulation and accompanying program of reference [16] to provide stable solutions for either free, partially restrained, or fully restrained boundaries.

In 1995, Smith [29] published his development of the formulation for the finite difference analysis of general open-ended rotationally symmetric shells under either static or time-dependent continuous loadings for which a variable nodal point spacing may be used in the meridional finite difference mesh. As in reference [19], the governing differential equations were formulated in terms of the displacements w, u_ϕ, and u_Θ and Fourier expansion was used in the circumferential direction of the shell. The complete system of equations is solved implicitly for the first time increment after using low order central difference variable nodal point spacing representations for all spatial derivatives and using ordinary time derivatives. Explicit relations are used to obtain the displacements w_n, $u_{\phi n}$, and $u_{\Theta n}$ within the boundary edges of the shell for the second and later time increments. The remaining fundamental variables are, for the second and later time increments, found from separate implicit solutions at each boundary. The selection of a time increment which, in conjunction with the spatial finite difference mesh, is expected to produce numerically stable solutions is obtained from an explicit empirical relation for the time increment in terms of the minimum spatial increment.

In 1997, Smith [30] published his development of improvements to the formulation and finite difference representations used in reference [9]. These improvements included the addition of inertia forces and applied loadings in the circumferential direction of the shell and incorporation of the meridional co-ordinate s as the spatial variable *in lieu* of the co-ordinate z along the axis of symmetry of the shell. Solution formulations by both the explicit method and the implicit method for time-dependent loadings are included. Solutions found by the two methods show favorable comparison.

In 1998, Smith [31] published a second report on the finite difference analysis of rotationally symmetric shells under either static or dynamic loadings for which a variable node point spacing may be used in the spatial finite difference mesh and for which an eigenvalue analysis of the explicit coefficient matrices to evaluate numerical stability (or instability) of the solution for given choices of spatial mesh and time increment for the case of dynamic loadings was incorporated. Additionally, the finite difference representation for second and fourth derivatives was altered from that used in reference [29] to provide a consistent order of truncation error for all derivatives, thus departing from a central derivative representation for second and fourth derivatives.

In summary of the above references, we note that the only publications dealing specifically with the analysis of thin isotropic general shells under either symmetric or non-symmetrical loads by the modal superposition method are reference [7] by Kraus and Kalnins, reference [14] by Radwan and Genin, and reference [18] by Chang *et al.* In reference [7], the frequencies and modes of free vibration are determined by the multi-segment direct numerical integration approach developed by Kalnins in references [4] and [6]. This segmentation of the shell into short segments to accomplish the direct numerical integration is due to loss of accuracy in the integration for shells which have a length of meridian factor β greater than 3–5 as determined experimentally [4]. In reference [14], introduction of the assumed, known, or calculated mode shape functions into LaGrange's equations of motion results in a system of ordinary differential equations for the generalized time co-ordinates. We note, however, that determination of the frequencies and mode shape functions is not given in reference [14]. It is merely indicated therein that these functions can be found by a finite element analysis. In reference [18], the solution for each Fourier harmonic is obtained by determining the natural frequencies and mode shapes by use of doubly curved axisymmetric shell finite elements followed by expansion of the solution in terms of the meridional mode shapes and time-dependent "modal participation factors". The solution for each Fourier component is given by a superposition of the several modal contributions. The total response is then given by a second summation of the separate solutions for the total number of Fourier components used to represent the loadings.

In this article, our purpose is to report procedures implemented by Smith [25] for determining the total shell response of any rotationally symmetric general shell, which may have variable thickness along the shell meridian, under time-dependent (or static) surface loadings by the modal superposition method as described previously in this introduction.

The use of ordinary finite difference representations for the derivatives in the governing differential equations formulated in terms of the displacements to determine the frequencies and mode shapes [19, 20] results in advantages over the methods used in references [7, 14, 18]. It avoids the necessity for multisegment direct numerical integration in reference [7] and the possible adverse effects of shear locking behaviour for thin shells [27, 32] for the finite element formulations of references [14, 18]. In contrast to solutions found by the finite difference energy method of references [12, 13], it also provides solutions for which continuity of all displacements and derivatives thereof exist at every node point in the finite difference mesh.

2. GOVERNING DIFFERENTIAL EQUATIONS

Our system of governing equations will be based on the linear classical theory of shells as given by Reissner [33]. Surface loadings and inertia forces in each of the displacement directions w, u_ϕ, and u_θ will be considered. All rotary inertia terms and thermal effects will

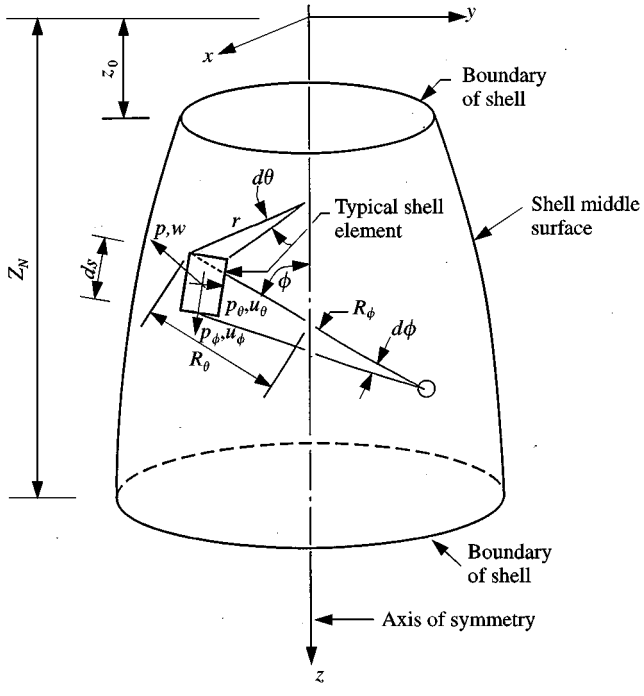

Figure 1. Typical shell of revolution.

be neglected. The thickness h of the shell may vary along the meridian, and we assume continuity of h and its derivatives through the second order. We assume that $\rho/R_\phi \ll 1$ and that $\rho/R_\theta \ll 1$. Hence, we take $N_{\theta\phi} = N_{\phi\theta}$ and $M_{\theta\phi} = M_{\phi\theta}$.

The geometry and co-ordinate system for the middle surface of our shell is shown in Figure 1. Shell element membrane and shear forces are shown in Figure 2, and shell element bending and twisting moments are shown in Figure 3.

We assume that the material of the shell is both homogeneous and isotropic. Inasmuch as we are not considering thermal loadings, the quantities E and v will remain constant. Thus, we assume that

$$E = \text{constant}, \qquad v = \text{constant}. \tag{1}$$

Our system of governing equations involving the stress–strain relations, strain–displacement relations, and the force equilibrium equations can be reduced to a system of equations consisting of three differential equations in terms of three unknown displacements w, u_ϕ, and u_θ. It will be convenient, however, to incorporate into our system of equations as unknowns at the boundary edges of the shell the remaining quantities which enter into the natural boundary conditions at $\phi = \text{constant}$. In the classical theory of shells, the quantities which appear in the natural boundary conditions on a rotationally symmetric edge of a shell of revolution are the generalized displacements w, u_ϕ, u_θ, and β_ϕ and the generalized forces Q, N_ϕ, N, and M_ϕ. Thus, our system of equations will consist of the three field equations in terms of the displacements w, u_ϕ, and u_θ and a definition of β_ϕ, Q, N_ϕ, N, and M_ϕ at each boundary in terms of the displacements w, u_ϕ, and u_θ together with four equations prescribing the appropriate four of the quantities w, u_ϕ, u_θ, β_ϕ, Q, N_ϕ, N, and

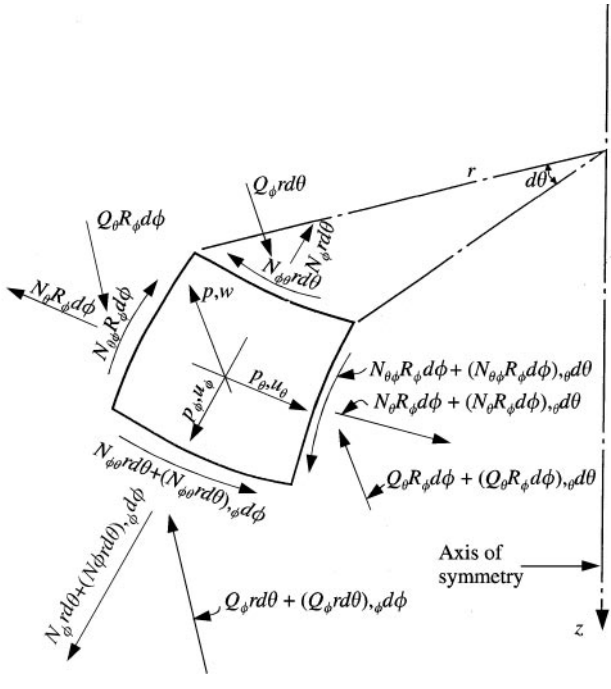

Figure 2. Shell element membrane and shear forces.

M_ϕ at each boundary of the shell. The quantities N and Q are the effective shear resultants and are defined as

$$N = N_{\theta\phi} + \frac{\sin\phi}{r} M_{\theta\phi}, \qquad Q = Q_\phi + \frac{1}{r} M_{\theta\phi,\theta}. \tag{2, 3}$$

We define the quantities w, u_ϕ, u_θ, β_ϕ, Q, N_ϕ, N, and M_ϕ to constitute the primary variables in our system of equations. The variables β_θ, N_θ, $N_{\theta\phi}$, M_θ, $M_{\theta\phi}$, Q_ϕ, and Q_θ are designated as the secondary variables. From two of our five useful equations of equilibrium, we find

$$Q_\phi = \frac{1}{r} M_{\theta\phi,\theta} + M_{\phi,s} + \frac{\cos\phi}{r}(M_\phi - M_\theta), \tag{4}$$

$$Q_\theta = \frac{1}{r} M_{\theta,\theta} + M_{\theta\phi,s} + \frac{2\cos\phi}{r} M_{\theta\phi}. \tag{5}$$

By substituting equations (4) and (5) into the remaining three equations of equilibrium, our three reduced equations of equilibrium in terms of the force variables thus become

$$N_{\theta\phi,\theta} + rN_{\phi,s} + (N_\phi - N_\theta)\cos\phi + \frac{1}{R_\phi} M_{\theta\phi,\theta} + \frac{r}{R_\phi} M_{\phi,s}$$

$$+ \frac{\cos\phi}{R_\phi}(M_\phi - M_\theta) + rp_\phi - \frac{\gamma hr}{g} u_{\phi,tt} = 0, \tag{6}$$

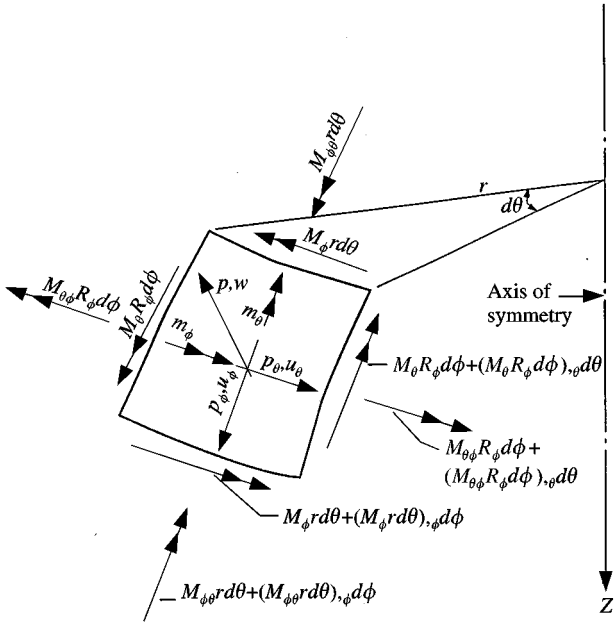

Figure 3. Shell element bending and twisting moments.

$$\frac{1}{r}M_{\theta,\theta\theta}+2M_{\theta\phi,\theta s}+\frac{2\cos\phi}{r}M_{\theta\phi,\theta}+rM_{\phi,ss}$$

$$+2\cos\phi M_{\phi,s}-\frac{\sin\phi}{R_\phi}(M_\phi-M_\theta)-\cos\phi M_{\theta,s}$$

$$-N_\theta\sin\phi-\frac{r}{R_\phi}N_\phi+rp-\frac{\gamma hr}{g}w_{,tt}=0, \tag{7}$$

$$N_{\theta,\theta}+rN_{\theta\phi,s}+2\cos\phi N_{\theta\phi}+\frac{\sin\phi}{r}M_{\theta,\theta}$$

$$+\sin\phi M_{\theta\phi,s}+\frac{2\sin\phi\cos\phi}{r}M_{\theta\phi}$$

$$+rp_\theta-\frac{\gamma hr}{g}u_{\theta,tt}=0. \tag{8}$$

To formulate our system of equations in terms of the displacements w, u_ϕ, and u_θ, we express the stress resultants N_θ, N_ϕ, $N_{\theta\phi}$, M_θ, M_ϕ, $M_{\theta\phi}$, N, and Q in terms of the displacements and substitute the appropriate quantities into the equations involving the force variables. This complete development may be found in reference [25].

The boundary conditions to be considered at the boundary s_0 are

$$w(s_0,\theta,t)=0 \quad \text{or} \quad Q(s_0,\theta,t)=0, \tag{9a}$$

$$u_\phi(s_0,\theta,t)=0 \quad \text{or} \quad N_\phi(s_0,\theta,t)=0, \tag{9b}$$

$$u_\theta(s_0, \theta, t) = 0 \quad \text{or} \quad N(s_0, \theta, t) = 0, \tag{9c}$$

$$\beta_\phi(s_0, \theta, t) = 0 \quad \text{or} \quad M_\phi(s_0, \theta, t) = 0, \tag{9d}$$

with similar boundary conditions at the boundary s_N.

For the initial conditions, we will prescribe initial values of the displacements and velocities in each of the displacement directions w, u_ϕ, and u_Θ. Thus, the initial conditions to be considered are typically

$$w(s, \theta, t_0) = w'(s, \theta, t_0), \qquad \dot{w}(s, \theta, t_0) = \dot{w}'(s, \theta, t_0), \tag{10a, b}$$

where the primed variables indicate specified values of the initial displacements and velocities. To solve our system of equations, we expand all loadings and dependent variables in the circumferential direction of the shell in Fourier series. The Fourier series representations of the loadings p_ϕ, p, the primary variables w, u_ϕ, β_ϕ, Q, N_ϕ, and M_ϕ, and the secondary variables N_θ, M_θ, and Q_ϕ are typically

$$p_\phi = \sum_{n=0}^{P} p_{\phi n}(s, t)\cos n\theta + \sum_{n=1}^{P} \bar{p}_{\phi n}(s, t)\sin n\theta. \tag{11a}$$

The loading p_θ, the primary variables u_θ and N, and the secondary variables β_θ, $N_{\theta\phi}$, $M_{\theta\phi}$, and Q_θ are typically

$$p_\theta = \sum_{n=1}^{P} p_{\theta n}(s, t)\sin n\theta + \sum_{n=0}^{P} \bar{p}_{\theta n}(s, t)\cos n\theta. \tag{11b}$$

Upon substituting equations (11) into our single system of equations involving θ, s, and t as the independent variables, we obtain $P + 1$ separate decoupled systems of equations in the variables s and t to solve *in lieu* of the single system of equations in the variables θ, s, and t. For each system we obtain two separate sets of equations, one for the variables which are designated without a bar and another for the variables which are designated with a bar. Here and elsewhere in the sequel where double signs occur in the equations, the upper sign is to accompany the first set of equations and the lower sign is to apply to the second set. Single signs will apply to both sets. The rather lengthy coefficients A_1–A_9, B_1–B_{12}, C_1–C_8, and D_1–D_{46}, which involve geometric and material parameters, loading terms, and the Fourier component designator n, appearing in the system of equations so found for each Fourier component may be found in reference [25].

With the referenced definition of coefficients, our field equations for each Fourier component of loading are given by

$$\begin{aligned} &- A_1 w_{n,sss} - A_2 w_{n,ss} + A_3 w_{n,s} + A_4 w_n \\ &+ A_5 u_{\phi n,ss} + A_6 u_{\phi n,s} + A_7 u_{\phi n} \pm A_8 u_{\theta n,s} \pm A_9 u_{\theta n} \\ &- \frac{\gamma h r}{g} u_{\phi n,tt} = - r p_{\phi n}, \end{aligned} \tag{12a}$$

$$- B_1 w_{n,ssss} - B_2 w_{n,sss} + B_3 w_{n,ss} + B_4 w_{n,s} + B_5 w_n$$

$$+ B_6 u_{\phi n,sss} + B_7 u_{\phi n,ss} + B_8 u_{\phi n,s} + B_9 u_{\phi n}$$

$$\pm B_{10} u_{\theta n,ss} \pm B_{11} u_{\theta n,s} \pm B_{12} u_{\theta n} - \frac{\gamma hr}{g} w_{n,tt} = - rp_n, \tag{12b}$$

$$\pm C_1 w_{n,ss} \pm C_2 w_{n,s} \mp C_3 w_n \mp C_4 u_{\phi n,s} \mp C_5 u_{\phi n}$$

$$+ C_6 u_{\theta n,ss} + C_7 u_{\theta n,s} + C_8 u_{\theta n} - \frac{\gamma hr}{g} u_{\theta n,tt} = - rp_{\theta n}. \tag{12c}$$

The primary variables $\beta_{\phi n}$, $N_{\phi n}$, $M_{\phi n}$, N_n, and Q_n in terms of the displacements are

$$\beta_{\phi n} = - w_{n,s} + \frac{1}{R_\phi} u_{\phi n}, \tag{13a}$$

$$N_{\phi n} = K(D_1 w_n + u_{\phi n,s} + D_2 u_{\phi n} \pm D_3 u_{\theta n}), \tag{13b}$$

$$M_{\phi n} = D(- w_{n,ss} - D_2 w_{n,s} + D_4 w_n + \frac{1}{R_\phi} u_{\phi n,s} + D_5 u_{\phi n} \pm D_6 u_{\theta n}), \tag{13c}$$

$$N_n = \pm D_{34} w_{n,s} \mp D_{35} w_n \mp D_{36} u_{\phi n} + D_{37} u_{\theta n,s} + D_{38} u_{\theta n}, \tag{13d}$$

$$Q_n = - Dw_{n,sss} - D_{39} w_{n,ss} + D_{40} w_{n,s} - D_{41} w_n + D_{42} u_{\phi n,ss}$$

$$+ D_{43} u_{\phi n,s} + D_{44} u_{\phi n} \pm D_{45} u_{\theta n,s} \pm D_{46} u_{\theta n}. \tag{13e}$$

The variables N_n and Q_n may also be given by

$$N_n = N_{\theta\phi n} + D_{33} M_{\theta\phi n}, \qquad Q_n = Q_{\phi n} + D_9 M_{\theta\phi n}. \tag{14a, b}$$

The secondary variables in terms of the displacements are

$$\beta_{\theta n} = \pm D_9 w_n + D_{33} u_{\theta n}, \tag{15a}$$

$$N_{\theta n} = K(D_7 w_n + v u_{\phi n,s} + D_8 u_{\phi n} \pm D_9 u_{\theta n}), \tag{15b}$$

$$M_{\theta n} = D\left(- v w_{n,ss} - D_8 w_{n,s} + D_{10} w_n + \frac{v}{R_\phi} u_{\phi n,s} + D_{11} u_{\phi n} \pm D_{12} u_{\theta n}\right), \tag{15c}$$

$$Q_{\phi n} = D\Bigg[- w_{n,sss} - D_{13} w_{n,ss} + D_{14} w_{n,s} - D_{15} w_n + \frac{1}{R_\phi} u_{\phi n,ss}$$

$$+ D_{16} u_{\phi n,s} + D_{17} u_{\phi n} \pm \frac{(1 + v) D_{12}}{2} u_{\theta n,s} \pm D_{18} u_{\theta n}\Bigg], \tag{15d}$$

$$N_{\theta\phi n} = D_{19}(\mp D_9 u_{\phi n} + u_{\theta n,s} - D_8 u_{\theta n}), \tag{15e}$$

$$M_{\theta\phi n} = D_{20}(\pm 2nw_{n,s} \mp 2D_{21}w_n \mp D_{22}u_{\phi n} + \sin\phi\, u_{\theta n,s} + D_{23}u_{\theta n}), \tag{15f}$$

$$Q_{\theta n} = D_{24}(\pm D_{25}w_{n,ss} \pm D_{26}w_{n,s} \mp D_{27}w_n \mp D_{28}u_{\phi n,s}$$

$$\mp D_{29}u_{\phi n} + D_{30}u_{\theta n,ss} + D_{31}u_{\theta n,s} + D_{32}u_{\theta n}). \tag{15g}$$

Equations (13) will be written for each boundary and incorporated into our system of equations for determining or defining w_n, $u_{\phi n}$, and $u_{\theta n}$ on the range of the variale s and $\beta_{\phi n}$, $N_{\phi n}$, $M_{\phi n}$, N_n, and Q_n at the boundaries of the shell. The remaining variables may then be found from equations (13)–(15).

The boundary conditions to be considered at the boundary s_0 for each Fourier harmonic are

$$w_n(s_0, t) = 0 \quad \text{or} \quad Q_n(s_0, t) = 0, \tag{16a}$$

$$u_{\phi n}(s_0, t) = 0 \quad \text{or} \quad N_{\phi n}(s_0, t) = 0, \tag{16b}$$

$$u_{\theta n}(s_0, t) = 0 \quad \text{or} \quad N_n(s_0, t) = 0, \tag{16c}$$

$$\beta_{\phi n}(s_0, t) = 0 \quad \text{or} \quad M_{\phi n}(s_0, t) = 0, \tag{16d}$$

with similar boundary conditions at s_N.

The initial conditions for each Fourier harmonic are typically

$$w_n(s, t_0) = w'_n(s, t_0), \qquad \dot{w}_n(s, t_0) = \dot{w}'_n(s, t_0), \tag{17a, b}$$

where the primed variables are specified quantities.

The system of equations (12)–(17) has been solved numerically by Smith [19, 20, 30] by use of ordinary spatial and temporal finite difference representations and by Smith [28] by use of high order spatial finite differences and ordinary temporal finite differences. Our purpose here is to present solutions by the modal superposition method as obtained by Smith [25], thus eliminating problems of numerical instability associated with references [19, 20, 28, 30].

3. FREQUENCIES AND NORMAL MODE SHAPES FOR THE nth FOURIER COMPONENT

For the field equations (12) subject to the homogeneous boundary conditions typified by equations (16), we envision a separate set of frequencies and mode shapes for each of the Fourier components used to represent the loadings. We will therefore develop our solutions for frequencies and normal mode shapes for the general Fourier component n. The three non-homogeneous field equations governing the shell response for the Fourier component n are given by equations (12). The frequencies and normal mode shapes may be obtained from the corresponding set of homogeneous field equations subject to appropriate homogeneous boundary conditions. Thus, with only the inertia forces acting on the shell, the homogeneous field equations will be

$$-A_1 w_{n,sss} - A_2 w_{n,ss} + A_3 w_{n,s} + A_4 w_n + A_5 u_{\phi n,ss}$$

$$+ A_6 u_{\phi n,s} + A_7 u_{\phi n} \mp A_8 u_{\theta n,s} \pm A_9 u_{\theta n} - \frac{\gamma hr}{g} u_{\phi n,tt} = 0, \tag{18a}$$

$$- B_1 w_{n,ssss} - B_2 w_{n,sss} + B_3 w_{n,ss} + B_4 w_{n,s} + B_5 w_n + B_6 u_{\phi n,sss}$$

$$+ B_7 u_{\phi n,ss} + B_8 u_{\phi n,s} + B_9 u_{\phi n} \pm B_{10} u_{\theta n,ss} \pm B_{11} u_{\theta n,s}$$

$$\pm B_{12} u_{\theta n} - \frac{\gamma h r}{g} w_{n,tt} = 0, \tag{18b}$$

$$\pm C_1 w_{n,ss} \pm C_2 w_{n,s} \mp C_3 w_n \mp C_4 u_{\phi n,s}$$

$$\mp C_5 u_{\phi n} + C_6 u_{\theta n,ss} + C_7 u_{\theta n,s} + C_8 u_{\theta n} - \frac{\gamma h r}{g} u_{\theta n,tt} = 0. \tag{18c}$$

We may separate the variables in equations (18) by assuming that

$$w_n = W_n(s) \cdot F(t), \qquad u_{\phi n} = U_{\phi n}(s) \cdot F(t), \qquad u_{\theta n} = U_{\theta n}(s) \cdot F(t), \tag{19}$$

where the functions $W_n(s)$, $U_{\phi n}(s)$, and $U_{\theta n}(s)$ represent the normal mode shapes and $F(t)$ represents the time variation of the normal mode free vibration.

If we substitute equations (19) into equations (18), we find

$$\ddot{F}(t) + \omega_n^2 F(t) = 0, \tag{20}$$

where $F(t)$ represents a periodic motion with a frequency of $\omega_n/2\pi$ and the separation constant ω_n is seen to be the circular frequency of free vibration of the shell for the Fourier component n in rad/s.

We find our three field equations governing free vibration of the shell for the nth Fourier component of loading to be

$$\frac{g}{\gamma h r} A_1 W_{n,sss} + \frac{g}{\gamma h r} A_2 W_{n,ss} - \frac{g}{\gamma h r} A_3 W_{n,s} - \frac{g}{\gamma h r} A_4 W_n$$

$$- \frac{g}{\gamma h r} A_5 U_{\phi n,ss} - \frac{g}{\gamma h r} A_6 U_{\phi n,s} - \left(\frac{g}{\gamma h r} A_7 + \omega_n^2 \right) U_{\phi n}$$

$$\mp \frac{g}{\gamma h r} A_8 U_{\theta n,s} \mp \frac{g}{\gamma h r} A_9 U_{\theta n} = 0, \tag{21a}$$

$$\frac{g}{\gamma h r} B_1 W_{n,ssss} + \frac{g}{\gamma h r} B_2 W_{n,sss} - \frac{g}{\gamma h r} B_3 W_{n,ss} - \frac{g}{\gamma h r} B_4 W_{n,s} - \left(\frac{g}{\gamma h r} B_5 + \omega_n^2 \right) W_n$$

$$- \frac{g}{\gamma h r} B_6 U_{\phi n,sss} - \frac{g}{\gamma h r} B_7 U_{\phi n,ss} - \frac{g}{\gamma h r} B_8 U_{\phi n,s} - \frac{g}{\gamma h r} B_9 U_{\phi n}$$

$$\mp \frac{g}{\gamma h r} B_{10} U_{\theta n,ss} \mp \frac{g}{\gamma h r} B_{11} U_{\theta n,s} \mp \frac{g}{\gamma h r} B_{12} U_{\theta n} = 0, \tag{21b}$$

$$\mp \frac{g}{\gamma hr} C_1 W_{n,ss} \mp \frac{g}{\gamma hr} C_2 W_{n,s} - \frac{g}{\gamma hr} C_3 W_n$$

$$\pm \frac{g}{\gamma hr} C_4 U_{\phi n,s} \pm \frac{g}{\gamma hr} C_5 U_{\phi n}$$

$$- \frac{g}{\gamma hr} C_6 U_{\theta n,ss} - \frac{g}{\gamma hr} C_7 U_{\theta n,s} - \left(\frac{g}{\gamma hr} C_8 + \omega_n^2 \right) U_{\theta n} = 0. \tag{21c}$$

In theory, equations (21) could be solved either in closed form or numerically, subject to appropriate boundary conditions, for the frequencies ω_{in} ($i = 1, 2, 3, \ldots, \infty$). We choose *in lieu* of a direct solution the use of the flexibility method of analysis for the discretized shell to be described subsequently.

To determine the frequencies ω_{mn} and the mode shapes Φ_{mn}, only the inertia forces will be acting on the shell. The boundary conditions to be considered are given by equations (16). We discretize the shell by dividing the shell meridian into N equal increments between the boundary at s_0 and the boundary at s_N. Thus, we will have $N + 1$ node points on the interval $s_0 \leqslant s \leqslant s_N$ together with additional node points beyond each boundary in our finite difference mesh for the discretized shell. We use this ordinary finite difference mesh to determine influence coefficients δ_{ij} for the shell by applying a total meridionally distributed unit loading for the Fourier component n at each of the $N + 1$ node points and in each of the co-ordinate directions w_n, $u_{\phi n}$, and $u_{\theta n}$ by use of the procedures contained in reference [19] and described in reference [20], which use equations (12) with inertia forces deleted and with application of appropriate loadings and boundary conditions. Details of this finite difference development for finding the influence coefficients δ_{ij} may be found in reference [25].

The dynamic displacements of the node points of the discretized shell are

$$\Delta_n(s, t) = [w_n(s_0, t), \ldots, w_n(s_N, t), u_{\phi n}(s_0, t), \ldots, u_{\phi n}(s_N, t), u_{\theta n}(s_0, t), \ldots, u_{\theta n}(s_N, t)]^{\mathrm{T}}. \tag{22}$$

The accelerations are

$$\ddot{\Delta}_n(s, t) = [\ddot{w}_n(s_0, t), \ldots, \ddot{w}_n(s_N, t), \ddot{u}_{\phi n}(s_0, t), \ldots, \ddot{u}_{\phi n}(s_N, t), \ddot{u}_{\theta n}(s_0, t), \ldots, \ddot{u}_{\theta n}(s_N, t)]^{\mathrm{T}}, \tag{23}$$

where the double dots over the displacement variables w_n, $u_{\phi n}$, and $u_{\theta n}$ indicate second derivatives with respect to time.

We lump the mass at the nodal point circles and note that in general the mass associated with any particular node point has three degrees of freedom, one in each of the three co-ordinate directions w_n, $u_{\phi n}$, and $u_{\theta n}$. The mass matrix M associated with each of the $N + 1$ node points along the meridian of the discretized shell is therefore a $3N + 3$ by $3N + 3$ diagonalized matrix with all off-diagonal elements equal to zero. Thus,

$$M = \frac{\gamma \Delta s}{r_0 g} [0{\cdot}5hr, hr, \ldots, hr, 0{\cdot}5hr, 0{\cdot}5hr, hr, \ldots, hr, 0{\cdot}5hr, 0{\cdot}5hr, hr, \ldots, hr, 0{\cdot}5hr]^D, \tag{24}$$

where the superscript D indicates a diagonalized matrix, γ is the weight of the shell material per unit volume, $h = h(s)$ along the shell meridian, r is the radius of the middle surface of the shell measured normal to the axis of symmetry, r_0 is the reference radius at the boundary s_0, and g is the gravitational acceleration constant.

The inertia force matrix F_n for the discretized shell is given by

$$F_n = M\ddot{\Delta}_n(s, t). \tag{25}$$

The dynamic displacements in equation (22) result from the inertia forces defined by equation (25). These displacements may be expressed by influence coefficients δ_{ij}, where δ_{ij} represents the displacement at node point i due to a total meridionally distributed unit loading for the Fourier component n at node point j. For shells with variable radius r, the matrix of influence coefficients δ_{ij} thus determined will not be symmetric since the circumferential loadings thus imposed vary linearly with r. To obtain our flexibility matrix, we require that the circumferential loading at each node point be constant. We choose to accomplish this by multiplying the coefficients δ_{ij} by the factor r_0/r_j to obtain

$$\delta = \left[\frac{r_0}{r_j}\,\delta_{ij}\right], \tag{26}$$

where r_j is the radius r of the middle surface of the shell at the node point j, and where

$$i = 1, \ldots, 3N + 3, \qquad j = 1, \ldots, 3N + 3.$$

The matrix of influence out coefficients δ thus determined consists of a $3N + 3$ by $3N + 3$ array of values which together constitute the flexibility matrix for the shell under the appropriate boundary conditions given by equation (16).

By applying D'Alembert's Principle, we obtain the equations of dynamic equilibrium for the nth Fourier component of the shell as

$$\Delta_n(s, t) = -\delta F_n. \tag{27}$$

To determine the normal modes of vibration, the initial displacements and velocities are zero. Thus, inasmuch as the free vibration of the shell has been shown to consist of a periodic motion with frequency ω_n, we may represent the displacements $\Delta_n(s, t)$ as

$$\Delta_n(s, t) = \sin \omega_n t \Delta_n(s), \tag{28}$$

where

$$\Delta_n(s) = [W_n(s_0), \ldots, W_n(s_N), U_{\phi n}(s_0), \ldots, U_{\phi n}(s_N),$$

$$U_{\theta n}(s_0), \ldots, (U_{\theta n}(s_N)])^{\mathrm{T}} \tag{29}$$

and where W_n, $U_{\phi n}$, and $U_{\theta n}$ represent the $3N + 3$ half amplitudes of free vibration at the $N + 1$ node points on the interval $s_0 \leqslant s \leqslant s_N$.

The accelerations in equations (23) will be given by

$$\ddot{\Delta}_n(s, t) = -\omega_n^2 \sin \omega_n t\, \Delta_n(s). \tag{30}$$

If we substitute equations (24) and (30) into equation (25), we have

$$F_n = -\frac{\gamma \Delta s \omega_n^2 \sin \omega_n t}{r_0 g}\,[0{\cdot}5hrW_n(s_0), hrW_n(s_1), \ldots, hrW_n(s_{N-1}),$$

$$0{\cdot}5hrW_n(s_N), 0{\cdot}5hrU_{\phi n}(s_0), hrU_{\phi n}(s_1), \ldots,$$

$$hrU_{\phi n}(s_{N-1}),\ 0{\cdot}5hrU_{\phi n}(s_N),\ 0{\cdot}5hrU_{\theta n}(s_0),$$

$$hrU_{\theta n}(s_1),\ \ldots,\ hrU_{\theta n}(s_{N-1}),\ 0{\cdot}5hrU_{\theta n}(s_N)]^{\mathrm{T}}. \tag{31}$$

If we substitute equations (26), (28), and (31) into equation (27) and cancel the common terms $\sin\omega_n t$ (since $\sin\omega_n t$ is not necessarily zero), we obtain

$$\frac{g}{\gamma\Delta s\omega_n^2}\,\Delta_n(s) = [\delta_{ij}][0{\cdot}5hW_n(s_0),\ hW_n(s_1),\ \ldots,\ hW_n(s_{N-1}),\ 0{\cdot}5hW_n(s_N),$$

$$0{\cdot}5hU_{\phi n}(s_0),\ hU_{\phi n}(s_1),\ \ldots,\ hU_{\phi n}(s_{N-1}),\ 0{\cdot}5hU_{\phi n}(s_N),$$

$$0{\cdot}5hU_{\theta n}(s_0),\ hU_{\theta n}(s_1),\ \ldots,\ hU_{\theta n}(s_{N-1}),\ 0{\cdot}5hU_{\theta n}(s_N)]^{\mathrm{T}}. \tag{32}$$

Equations (32) are the flexibility equations for the discretized shell. These equations can be rewritten in the form

$$(A - \lambda_{mn}\mathrm{I})\,\Phi_{mn} = 0, \tag{33}$$

where

$$\left.\begin{aligned} &A = [a_{ij}] \\ &a_{ij} = \frac{h(s_0)}{2}\,\delta_{ij}, \quad (j = 1,\ N+2,\ 2N+3) \\ &a_{ij} = \frac{h(s_N)}{2}\,\delta_{ij} \quad (j = N+1,\ 2N+2,\ 3N+3) \\ &\qquad\qquad (j = 2,\ \ldots,\ N; \\ &a_{ij} = h(s)\delta_{ij} \qquad j = N+3,\ \ldots,\ 2N+1; \\ &\qquad\qquad j = 2N+4,\ \ldots,\ 3N+2) \end{aligned}\right\} (i = 1,\ 2,\ 3,\ \ldots,\ 3N+3), \tag{34}$$

$$\lambda_{mn} = \frac{g}{\gamma\Delta s\omega_{mn}^2}, \qquad \omega_{mn} = \left(\frac{g}{\lambda_{mn}\gamma\Delta s}\right)^{1/2}, \tag{35}$$

$$\Phi_{mn} = [W_{mn}(s_0),\ \ldots,\ W_{mn}(s_N),\ U_{\phi mn}(s_0),\ \ldots,\ U_{\phi mn}(s_N),\ U_{\theta mn}(s_0),\ \ldots,\ U_{\theta mn}(s_N)]^{\mathrm{T}}, \tag{36}$$

I is the unit matrix with $3N + 3$ diagonal elements, and the first subscript m on all variables is associated with the mth eigenvalue for the Fourier component n.

In practice, when we specify $M (M = 3\,min$ to $6\,max)$ of the displacements $w_n(s_0, t)$, $u_{\phi n}(s_0, t)$, $u_{\theta n}(s_0, t)$, $w_n(s_N, t)$, $u_{\phi n}(s_N, t)$, and $u_{\theta n}(s_N, t)$ to be zero, we will obtain for the rows and columns of equations (33) M rows and M columns which will be zero. Before solving for the eigenvalues and eigenvectors associated with equations (33), we will condense the coefficient matrix to a $3N + 3 - M$ by $3N + 3 - M$ matrix and the displacement vector to a $3N + 3 - M$ column matrix. Thus, we will have only $3N + 3 - M$ values of ω_n corresponding to the $3N + 3 - M$ degrees of freedom of the shell.

The system of equations (33) has non-trivial solutions if and only if the determinant of the coefficient matrix for Φ_{mn} vanishes. Thus,

$$|A - \lambda_{mn} I| = 0 \tag{37}$$

is our frequency equation for the $3N + 3 - M$ values of λ_{mn} and subsequent determination of the $3N + 3 - M$ mode shapes.

After solution of equation (37) for our $3N + 3 - M$ eigenvalues λ_{mn} and mode shapes, the frequencies ω_{mn} will be found from equations (35). We expect $3N + 3 - M$ real and positive values of ω_{mn} to correspond to the $3N + 3 - M$ degrees of freedom of the shell. The eigenvalues and eigenvectors of equation (37) will be evaluated by a convergent iterative procedure which will determine successively the $3N + 3 - M$ real values of each. These quantities will be found by use of a standard subroutine given in reference [25] and credited to others therein.

4. PROPERTIES OF THE NORMAL MODE SHAPES

By analogy with equation (31), we define the characteristic loading for the mth mode to be the static loading q_{mn} expressed in terms of the mode shape functions Φ_{mn} as

$$q^i_{mn} = \omega^2_{mn} M^i \Phi^i_{mn} (i = 1, 2, 3, \ldots, 3N + 3), \tag{38}$$

where Φ_{mn} is given by equation (36).

It may be shown [25, 26] that, for any two mode shape functions Φ_{mn} and Φ_{kn},

$$\sum_{i=1}^{i=3N+3} M^i \Phi^i_{mn} \Phi^i_{kn} = 0 \quad (m \neq k). \tag{39}$$

Equation (39) is the equation of orthogonality between any two normal modes.

If $m = k$,

$$\sum_{i=1}^{i=3N+3} M^i (\Phi^i_{mn})^2 = \text{ANY CONSTANT}. \tag{40}$$

We normalize the mode shape functions Φ_{mn} by setting the constant in equation (40) equal to unity and designate the normalized function for the mth mode shape as $\bar{\Phi}_{mn}$. Thus, our normalizing condition is

$$\sum_{i=1}^{i=3N+3} M^i (\bar{\Phi}^i_{mn})^2 = 1. \tag{41}$$

After normalization of the mode shapes $\bar{\Phi}_{mn}$ in accordance with equation (41), we designate the normalized characteristic loading Q_{mn} to be

$$Q^i_{mn} = \omega^2_{mn} M^i \bar{\Phi}^i_{mn} \quad (i = 1, 2, 3, \ldots, 3N + 3). \tag{42}$$

Static deflections due to Q_{mn} will be given by

$$\Delta_{mn}(s) = \delta Q_{mn}. \tag{43}$$

If we substitute equations (26) and (42) into equation (43), we find equation (32), with the normalized mode shapes $\bar{\Phi}_{mn}$ appearing on both sides of the equation *in lieu* of the half-amplitudes appearing therein. Thus, it is seen that the static loading given by equation (42) produces the deflections $\bar{\Phi}_{mn}$ which constitute the normalized shapes of the mth vibration mode of the shell.

5. REPRESENTATION OF STATIC LOADINGS BY SUPERPOSITION OF NORMALIZED CHARACTERISTIC LOADINGS

We designate the static nodal point loading due to the loadings $p_n(s)$, $p_{\phi n}(s)$, and $p_{\theta n}(s)$ applied over the interval $s_0 \leqslant s \leqslant s_N$ as

$$P_n(s) = \frac{\Delta s}{r_0}\,[0{\cdot}5p_n(s_0)r_0,\, p_n(s_1)r_1, \ldots, p_n(s_{N-1})r_{N-1},$$
$$0{\cdot}5p_n(s_N)r_N, 0{\cdot}5p_{\phi n}(s_0)r_0,\, p_{\phi n}(s_1)r_1, \ldots,$$
$$p_{\phi n}(s_{N-1})r_{N-1},\, 0{\cdot}5p_{\phi n}(s_N)r_N,\, 0{\cdot}5p_{\theta n}(s_0)r_0,$$
$$p_{\theta n}(s_1)r_1, \ldots, p_n(s_{N-1})r_{N-1},\, 0{\cdot}5p_{\theta n}(s_N)r_N]^{\mathrm{T}}. \tag{44}$$

We wish to represent the loading $P_n(s)$ as a superposition of the appropriate contributions of the loadings given by equation (42). Thus, if we let ψ_{mn} represent the participation factor for mode m for the nth Fourier component of loading, we may represent the loading at any co-ordinate location i as

$$P_n^i = \sum_{m=1}^{m=3N+3-M} \psi_{mn} Q_{mn}^i \quad (i = 1, 2, 3, \ldots, 3N + 3). \tag{45}$$

It can be shown [25, 26] that

$$\psi_{mn} = \frac{\sum_{i=1}^{i=3N+3} P_n^i \bar{\Phi}_{mn}^i}{\omega_{mn}^2}. \tag{46}$$

6. DYNAMIC RESPONSE UNDER IMPULSIVE LOADINGS FOR THE nth FOURIER COMPONENT

The dynamic response of the shell under impulsive loadings will be determined by a superposition of the several modal contributions. For this purpose, we assume that the initial displacements and velocities are zero and that the impulsive loadings $p_n(s, t)$, $p_{\phi n}(s, t)$, and $p_{\theta n}(s, t)$ vary with time in the same manner throughout the interval $s_0 \leqslant s \leqslant s_N$ of the shell.

It has been shown by Norris *et al.* [26] that the total response due to initial displacements and velocities in conjunction with impulsively applied forces may be determined by independently evaluating the response due to initial displacements and velocities and the response due to the impulsive forces and superimposing the results. We thus consider first the response due to impulsive loadings and will subsequently evaluate the response due to initial displacements and velocities.

We designate the time-dependent nodal point impulsive loading due to the loadings $p_n(s, t)$, $p_{\phi n}(s, t)$, and $p_{\theta n}(s, t)$ applied over the interval $s_0 \leqslant s \leqslant s_N$ as

$$P_n(s, t) = P_n(s) f(t), \tag{47}$$

where the $P_n(s)$ represent the maximum instantaneous values attained by the dynamic loading and where $f(t)$ is the time function defining the temporal variation of the loading.

By analogy with equation (45), we represent the time-dependent loadings in equation (47) by

$$P_n^{(i,t)} = \sum_{m=1}^{m=3N+3-M} f(t)\psi_{mn} Q_{mn}^i \quad (i = 1, 2, 3, \ldots, 3N + 3). \tag{48}$$

From equations (32), (43), and (45), it can be seen that the static loading given by equation (45) produces the deflections

$$\Delta_n^i = \sum_{m=1}^{m=3N+3-M} \psi_{mn} \bar{\Phi}_{mn}^i \quad (i = 1, 2, 3, \ldots, 3N + 3) \tag{49}$$

at each of the co-ordinate locations i on the shell meridian. We may similarly represent the dynamic deflections $\Delta_n^{(i,t)}$ under the loadings given by equation (48) as

$$\Delta_n^{(i,t)} = \sum_{m=1}^{m=3N+3-M} \eta_{mn}(t)\psi_{mn} \bar{\Phi}_{mn}^i \quad (i = 1, 2, 3, \ldots, 3N + 3), \tag{50}$$

where the dynamic load factors $\eta_{mn}(t)$ are to be determined for each mode m. Similar summations with the appropriate upper limits may be used to obtain the dynamic displacements for the symmetric and antisymmetric components of loading for the Fourier component $n = 0$.

7. MODAL DYNAMIC LOAD FACTORS FOR IMPULSIVE LOADINGS

To determine the dynamic load factor $\eta_{mn}(t)$, we consider the dynamic equilibrium of the shell under the impulsive loadings given by equation (48) and the inertia forces $M^i \ddot{\Delta}_n^{(i,t)}$, where M^i is given by equation (24) and where the displacements $\Delta_n^{(i,t)}$ are represented by equation (50). By also writing the displacements $\Delta_n^{(i,t)}$ in terms of the influence coefficients δ_{ij} for the shell as utilized previously in equation (27) and by applying D'Alembert's Principle, we find the equations for the dynamic displacements $\Delta_n^{(i,t)}$ at the several node points i of the shell to be

$$[\Delta_n^{(i,t)}] = [\delta][P_n^{(j,t)} - M^j \ddot{\Delta}_n^{(j,t)}] \qquad (i = 1, 2, 3, \ldots, 3N + 3;\ j = 1, 2, 3, \ldots, 3N + 3). \tag{51}$$

By substituting equations (42), (48), and (50) into equation (51), we have

$$\sum_{m=1}^{m=3N+3-M} [\delta][f(t)\psi_{mn}\omega_{mn}^2 M^j \bar{\Phi}_{mn}^j - \psi_{mn}\ddot{\eta}_{mn} M^j \bar{\Phi}_{mn}^j]$$

$$- \sum_{m=1}^{m=3N+3-M} \eta_{mn}\psi_{mn}\bar{\Phi}_{mn}^i = 0 \qquad (i = 1, 2, 3, \ldots, 3N + 3;\ j = 1, 2, 3, \ldots, 3N + 3). \tag{52}$$

From equation (32), however, we obtain

$$\frac{1}{\omega_{mn}^2}[\bar{\Phi}_{mn}^i] = [\delta][M^j\bar{\Phi}_{mn}^j] \qquad (i = 1, 2, 3, \ldots, 3N + 3;\ j = 1, 2, 3, \ldots, 3N + 3). \quad (53)$$

By substituting equation (53) into equation (52), we find

$$\sum_{m=1}^{m=3N+3-M}\left[f(t)\psi_{mn}\bar{\Phi}_{mn}^i - \frac{\ddot{\eta}_{mn}\psi_{mn}\bar{\Phi}_{mn}^i}{\omega_{mn}^2} - \eta_{mn}\psi_{mn}\bar{\Phi}_{mn}^i\right] = 0 \qquad (i = 1, 2, 3, \ldots, 3N + 3). \quad (54)$$

By multiplying equation (54) by the quantity $\bar{\Phi}_{kn}^i M^i$ for the kth general mode and summing the resulting $3N + 3$ equations, we obtain

$$\sum_{i=1}^{i=3N+3}\sum_{m=1}^{m=3N+3-M}\left[f(t)\psi_{mn}\bar{\Phi}_{kn}^i\bar{\Phi}_{mn}^i M^i - \frac{\ddot{\eta}_{mn}\psi_{mn}\bar{\Phi}_{kn}^i\bar{\Phi}_{mn}^i M^i}{\omega_{mn}^2} - \eta_{mn}\psi_{mn}\bar{\Phi}_{kn}^i\bar{\Phi}_{mn}^i M^i\right] = 0$$

$$(i = 1, 2, 3, \ldots, 3N + 3;\ j = 1, 2, 3, \ldots, 3N + 3 - M). \quad (55)$$

By virtue of equations (39) and (41), the double sum in equation (55) reduces to

$$\ddot{\eta}_{mn} + \omega_{mn}^2\eta_{mn} = \omega_{mn}^2 f(t). \quad (56)$$

The solution of equation (56) is

$$\eta_{mn}(t) = \omega_{mn}\int_{t_0}^{t} f(\tau)\sin\omega_{mn}(t - \tau)\,\mathrm{d}\tau, \quad (57)$$

where $f(\tau)$ is used to define the temporal variation of the loading.

With the $\bar{\Phi}_{mn}^i$ determined from equation (41), the ψ_{mn} found from equation (46), and with η_{mn} found from equation (57), we may evaluate the Fourier components of the dynamic displacements $\Delta_n^{(i,t)}$ in the absence of initial displacements and velocities from equation (50). The velocities $\dot{\Delta}_n^{(i,t)}$ and the accelerations $\ddot{\Delta}_n^{(i,t)}$ may be found by appropriate differentiations of $\eta_{mn}(t)$ and using the resulting expressions found from equation (50).

8. DYNAMIC RESPONSE DUE TO INITIAL DISPLACEMENTS AND VELOCITIES FOR THE nth FOURIER COMPONENT

The development of the system of equations (50) for the dynamic displacements $\Delta_n^{(i,t)}$ was based on the assumption of zero values for the initial displacements and velocities at all node points i along the shell meridian. The solution for the time-dependent displacements $\Delta_{In}^{(i,t)}$ due to initial displacements $\Delta_{In}^{(i,t_0)}$ and initial velocities $\dot{\Delta}_{In}^{(i,t_0)}$ other than zero remains to be determined for addition to the already determined $\Delta_n^{(i,t)}$ caused by only the impulsive loadings $P_n^{(i,t)}$ to determine the total time-dependent displacements $\Delta_{Tn}^{(i,t)}$ due to the combined effects of impulsive loadings and initial displacements and velocities. Thus, we represent the total displacements $\Delta_{Tn}^{(i,t)}$ as

$$\Delta_{Tn}^{(i,t)} = \Delta_n^{(i,t)} + \Delta_{In}^{(i,t)} \quad (i = 1, 2, 3, \ldots, 3N + 3). \quad (58)$$

We represent the column vector of displacement $\Delta_{In}^{(i,t)}$ by the right-hand side of equation (22). The velocities $\dot{\Delta}_{In}^{(i,t)}$ and the accelerations $\ddot{\Delta}_{In}^{(i,t)}$ will be given by appropriate differentiations of the right-hand sides of equation (22).

For any time $t \geqslant t_0$, the inertia forces acting on the shell will, in the absence of impulsive loadings, be given by

$$F_{In}^{(i,t)} = M\ddot{\Delta}_{In}^{(i,t)}, \tag{59}$$

where the diagonalized mass matrix M is given by equation (24).

If we neglect damping, the only forces causing the deflections $\Delta_{In}^{(i,t)}$ in equation (58) will be the inertia forces $F_{In}^{(i,t)}$ given by equation (59). It is clear from equations (27) and (32) that the dynamic displacements $\Delta_{In}^{(i,t)}$ may thus be represented by a superposition of the normalized mode shapes $\bar{\Phi}_{mn}^{i}$ multiplied by a suitable time function $\eta_{mn}^{I}(t)$. Thus, we represent the dynamic displacements $\Delta_{In}^{(i,t)}$ as

$$\Delta_{In}^{(i,t)} = \sum_{m=1}^{m=3N+3-M} \eta_{mn}^{I}(t)\,\bar{\Phi}_{mn}^{i} \quad (i = 1, 2, 3, \ldots, 3N + 3), \tag{60}$$

where the time functions $\eta_{mn}^{I}(t)$ are yet to be determined for each mode m.

The velocities $\dot{\Delta}_{In}^{(i,t)}$ and the accelerations $\ddot{\Delta}_{In}^{(i,t)}$ will be given by appropriate differentiations of $\eta_{mn}^{I}(t)$ and using the resulting expressions found from equation (60).

By a development similar to that used in sections 6 and 7 for impulsive loadings, which may be found in reference [25], we find

$$\eta_{mn}^{I}(t) = \eta_{mn}^{I}(t_0)\cos\omega_{mn}(t - t_0) + \frac{\dot{\eta}_{mn}^{I}(t_0)}{\omega_{mn}}\sin\omega_{mn}(t - t_0), \tag{61}$$

$$\eta_{mn}^{I}(t_0) = \sum_{i=1}^{i=3N+3} M^{i}\bar{\Phi}_{mn}^{i}\Delta_{In}^{(i,t_0)}, \qquad \dot{\eta}_{mn}^{I}(t_0) = \sum_{i=1}^{i=3N+3} M^{i}\bar{\Phi}_{mn}^{i}\dot{\Delta}_{In}^{(i,t_0)}. \tag{62, 63}$$

With $\bar{\Phi}_{mn}^{i}$ found from equation (41) and $\eta_{mn}^{I}(t)$ given by equation (61), the dynamic displacements $\Delta_{In}^{(i,t)}$ due to the initial displacements and velocities of the shell will be found from equation (60) for the nth Fourier component of response.

The velocities $\dot{\Delta}_{In}^{(i,t)}$ and accelerations $\ddot{\Delta}_{In}^{(i,t)}$ will be found by appropriate differentiations of equation (60) and use of the resulting expressions. Similar expressions, with appropriate change of limits, may be used to obtain the displacements, velocities, and accelerations for the Fourier component $n = 0$.

9. TOTAL DYNAMIC DISPLACEMENTS UNDER COMBINED IMPULSIVE LOADINGS, INITIAL DISPLACEMENTS, AND INITIAL VELOCITIES

The solutions discussed previously will be obtained for each of the several Fourier components used to define the loadings and the initial displacements and velocities over the middle surface of the shell. The total dynamic response of the shell at any time t will consist of a double summation of the separate contributions, $3N + 3 - M$ contributions for each separate Fourier component n and $P + 1$ values for the several Fourier components n, where P is the highest Fourier number used to represent the loadings and the initial displacements and velocities. It should be noted also that, although the equations developed

hereinbefore have been written by utilizing the symmetric Fourier components of loadings and displacements, similar equations with appropriate variables and signs are applicable to the antisymmetric components. The nth Fourier components of displacements due to combined impulsive loadings and initial displacements and velocities will be given by equation (58), together with a similar equation for the antisymmetric components. Similar equations, with appropriate changes in limits, will be used to find the displacements for $n = 0$.

By observing equation (58) and the correspondence given in equations (22) and (50) between the $\Delta_n^{(i,t)}$ and $\Delta_{In}^{(i,t)}$ and the displacements $w_n(s, t)$, $u_{\phi n}(s, t)$, and $u_{\theta n}(s, t)$, we may now determine the displacements $w(s, \theta, t)$, $u_\phi(s, \theta, t)$, and $u_\theta(s, \theta, t)$ by use of the appropriate variables in equations (11).

10. FINITE DIFFERENCE RELATIONS FOR VARIABLES OTHER THAN DISPLACEMENTS

The symmetric Fourier components of the displacements due to combined impulsive loadings and initial conditions are given as $\Delta_{Tn}^{(i,t)}$ by equation (58). The column vectors of these time-dependent Fourier components of the displacements are identified in terms of the symmetric displacement components $w_n(s, t)$, $u_{\phi n}(s, t)$, and $u_{\theta n}(s, t)$ by equations (22) and (50). Similar equations define the antisymmetric Fourier components. The remaining variables of interest are the primary variables $\beta_{\phi n}$, $N_{\phi n}$, $M_{\phi n}$, N_n, and Q_n and the secondary variables $\beta_{\theta n}$, $N_{\theta n}$, $M_{\theta n}$, $Q_{\phi n}$, $N_{\theta\phi n}$, $M_{\theta\phi n}$, and $Q_{\theta n}$ (with it being understood here and elsewhere that the barred variables are included as well) on the interval $s_0 \leqslant s \leqslant s_N$. The primary variables are given by equations (13), while the secondary variables are given by equations (15).

Details of the finite difference development for finding the Fourier components of the above primary and secondary variables may be found in reference [25]. With these Fourier components known, the total time-dependent quantities may be found by use of the appropriate variables in equations (11).

11. RESULTS

To illustrate the utility of the program in reference [25], we include here solutions for a parabolic shell and compare the solutions obtained by the modal superposition method with solutions found numerically by the method of finite temporal differences as developed in references [19, 20]. The geometry and loading for our example parabolic shell are shown in Figure 4. We assume the initial displacements and velocities to be zero. For the boundary conditions, we assume that w, u_ϕ, β_ϕ, and u_θ are zero at s_0 and that Q, N_ϕ, M_ϕ, and N are zero at s_N. We assume a value of 30×10^6 lb/in^2 for E, a value of 0·2835 lb/in^3 for γ, and a value of 0·30 for v. We use for illustration only the Fourier components for $n = 0$–8. The six non-zero components entering into the solution are $p_0 = -31{\cdot}8$, $p_1 = -50{\cdot}0$, $p_2 = -21{\cdot}2$, $p_4 = 4{\cdot}2$, $p_6 = -1{\cdot}8$ and $p_8 = 1{\cdot}0$ lb/in^2. We specify 72 equal increments Δs along the shell meridian from s_0 to s_N.

By using the computer program in reference [25], we obtain the frequencies and their corresponding normalized mode shapes. We also obtain values of the summed Fourier series for all primary and secondary variables at all 73 node points from s_0 to s_N along the meridian of the shell for our selection of 10 equally spaced times varying from $t = 0{\cdot}12 \times 10^{-3}$ s to $t = 1{\cdot}20 \times 10^{-3}$ s. We show in Table 1 the values of $w(s_N, t)$, $u_\phi(s_N, t)$,

TABLE 1

Example parabolic shell solutions for $w(s_N, t)$, $u_\phi(s_N, t)$, $Q(s_0, t)$, and $N_\phi(s_0, t)$ at $\theta = 0$ by the modal superposition method with $\Delta s = 0{\cdot}3220$ in

$t(10^{-3}$ s)	$w(s_N, t)$ (in)	$u_\phi(s_N, t)$(in)	$Q(s_0, t)$(lb/in)	$N_\phi(s_0, t)$(lb/in)
0	0	0	0	0
0·12	$-9{\cdot}2254 \times 10^{-3}$	$7{\cdot}4603 \times 10^{-5}$	$-9{\cdot}8818 \times 10^{1}$	$7{\cdot}8737 \times 10^{2}$
0·24	$-3{\cdot}2699 \times 10^{-2}$	$-3{\cdot}5930 \times 10^{-4}$	$-6{\cdot}0753 \times 10^{1}$	$2{\cdot}4942 \times 10^{3}$
0·36	$-6{\cdot}5411 \times 10^{-2}$	$-3{\cdot}5375 \times 10^{-3}$	$-6{\cdot}8868 \times 10^{1}$	$3{\cdot}8688 \times 10^{3}$
0·48	$-1{\cdot}0253 \times 10^{-1}$	$-9{\cdot}3077 \times 10^{-3}$	$-7{\cdot}4672 \times 10^{1}$	$5{\cdot}0897 \times 10^{3}$
0·60	$-1{\cdot}3674 \times 10^{-1}$	$-1{\cdot}4038 \times 10^{-2}$	$-6{\cdot}4719 \times 10^{1}$	$6{\cdot}6498 \times 10^{3}$
0·72	$-1{\cdot}6372 \times 10^{-1}$	$-1{\cdot}6997 \times 10^{-2}$	$-6{\cdot}3864 \times 10^{1}$	$8{\cdot}2476 \times 10^{3}$
0·84	$-1{\cdot}8657 \times 10^{-1}$	$-2{\cdot}0668 \times 10^{-2}$	$-6{\cdot}1417 \times 10^{1}$	$9{\cdot}0884 \times 10^{3}$
0·96	$-2{\cdot}0499 \times 10^{-1}$	$-2{\cdot}2745 \times 10^{-2}$	$-6{\cdot}0946 \times 10^{1}$	$9{\cdot}7849 \times 10^{3}$
1·08	$-2{\cdot}1787 \times 10^{-1}$	$-2{\cdot}0530 \times 10^{-2}$	$-5{\cdot}4391 \times 10^{1}$	$1{\cdot}0697 \times 10^{4}$
1·20	$-2{\cdot}2197 \times 10^{-1}$	$-1{\cdot}9175 \times 10^{-2}$	$-2{\cdot}0805 \times 10^{1}$	$1{\cdot}0487 \times 10^{4}$

TABLE 2

Example parabolic shell solutions for $w(s, t)$, $u_\phi(s, t)$, at $\theta = 0$ by the modal superposition method with $\Delta s = 0{\cdot}3220$ in and $t = 1{\cdot}20 \times 10^{-3}$ s

s(in)	$w(s, t)$(in)	$u_\phi(s, t)$(in)
0·00	0	0
1·93	$-1{\cdot}2048 \times 10^{-2}$	$5{\cdot}3845 \times 10^{-3}$
3·86	$-2{\cdot}6975 \times 10^{-2}$	$9{\cdot}0794 \times 10^{-3}$
5·79	$-4{\cdot}0108 \times 10^{-2}$	$1{\cdot}1128 \times 10^{-2}$
7·72	$-6{\cdot}0163 \times 10^{-2}$	$1{\cdot}1637 \times 10^{-2}$
9·66	$-8{\cdot}4210 \times 10^{-2}$	$1{\cdot}0640 \times 10^{-2}$
11·59	$-1{\cdot}0305 \times 10^{-1}$	$8{\cdot}3733 \times 10^{-3}$
13·52	$-1{\cdot}2011 \times 10^{-1}$	$5{\cdot}1228 \times 10^{-3}$
15·45	$-1{\cdot}3807 \times 10^{-1}$	$1{\cdot}1645 \times 10^{-3}$
17.38	$-1{\cdot}6070 \times 10^{-1}$	$-3{\cdot}3538 \times 10^{-3}$
19·32	$-1{\cdot}8525 \times 10^{-1}$	$-8{\cdot}3291 \times 10^{-3}$
21·25	$-2{\cdot}0546 \times 10^{-1}$	$-1{\cdot}3653 \times 10^{-2}$
23·18	$-2{\cdot}2197 \times 10^{-1}$	$-1{\cdot}9175 \times 10^{-2}$

$Q(s_0, t)$, and $N_\phi(s_0, t)$ for the meridian $\theta = 0$ for each of the 10 selected times. We show in Table 2 values of $w(s, t)$ and $u_\phi(s, t)$ for the meridian $\theta = 0$ at all node points 6 Δs in apart between s_0 and s_N at time $t = 1{\cdot}20 \times 10^{-3}$ s.

To compare solutions by the modal superposition method with those found by the temporal finite difference method, we will solve the same parabolic shell example shown in Figure 4 by the program given in reference [19]. By using $\Delta s = 0{\cdot}3220$ in and $\Delta t = 0{\cdot}15 \times 10^{-5}$ s, we develop our solutions at all node points for our selection of 10 equally spaced times varying from $t = 0{\cdot}12 \times 10^{-3}$ to $1{\cdot}20 \times 10^{-3}$ s. We show in Table 3 the values of $w(s_N, t)$, $u_\phi(s_N, t)$, $Q(s_0, t)$, and $N_\phi(s_0, t)$ for the meridian $\theta = 0$ for each of the 10 selected times. We list in Table 4 values of $w(s, t)$ and $u_\phi(s, t)$ for the meridian $\theta = 0$ at all node points 6 Δs in apart between s_0 and s_N at time $t = 1{\cdot}20 \times 10^{-3}$ s. It is seen from Tables 1–4 that the solutions obtained for the example parabolic shell by the modal superposition

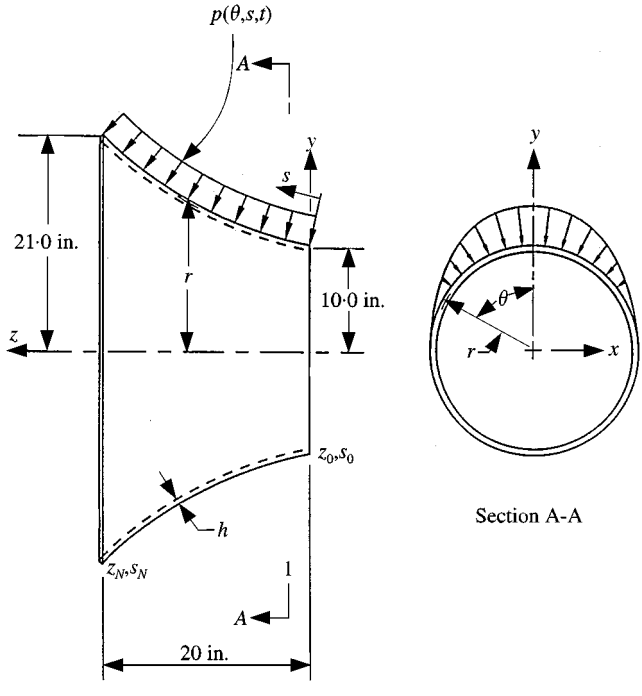

Figure 4. Example parabolic shell with suddenly applied cosine loading. The loading $p(\theta, s, t) = -100\cos\theta(-\pi/2 \leqslant \theta \leqslant \pi/2)$. The radius $r = 10 + 0{\cdot}15z + 0{\cdot}02z^2$. The boundary at s_0 is completely fixed, and the boundary at s_N is completely free. The thickness $h = 0{\cdot}10$ in.

TABLE 3

Example parabolic shell solutions for $w(s_N, t)$, $u_\phi(s_N, t)$, $Q(s_0, t)$, and $N_\phi(s_0, t)$ at $\theta = 0$ by the temporal finite difference method with $\Delta s = 0{\cdot}3220$ in and $\Delta t = 0{\cdot}15 \times 10^{-5}$ s

$t(10^{-3}\,\mathrm{s})$	$w(s_N, t)$ (in)	$u_\phi(s_N, t)$(in)	$Q(s_0, t)$(lb/in)	$N_\phi(s_0, t)$(lb/in)
0	0	0	0	0
0·12	$-9{\cdot}2243 \times 10^{-3}$	$7{\cdot}5403 \times 10^{-5}$	$-9{\cdot}1698 \times 10^{1}$	$7{\cdot}7092 \times 10^{2}$
0·24	$-3{\cdot}2757 \times 10^{-2}$	$-3{\cdot}5587 \times 10^{-4}$	$-6{\cdot}0106 \times 10^{1}$	$2{\cdot}4902 \times 10^{3}$
0·36	$-6{\cdot}5502 \times 10^{-2}$	$-3{\cdot}5348 \times 10^{-3}$	$-6{\cdot}4980 \times 10^{1}$	$3{\cdot}8639 \times 10^{3}$
0·48	$-1{\cdot}0260 \times 10^{-1}$	$-9{\cdot}3058 \times 10^{-3}$	$-7{\cdot}0207 \times 10^{1}$	$5{\cdot}0821 \times 10^{3}$
0·60	$-1{\cdot}3677 \times 10^{-1}$	$-1{\cdot}4035 \times 10^{-2}$	$-5{\cdot}9294 \times 10^{1}$	$6{\cdot}6444 \times 10^{3}$
0·72	$-1{\cdot}6376 \times 10^{-1}$	$-1{\cdot}6999 \times 10^{-2}$	$-5{\cdot}7579 \times 10^{1}$	$8{\cdot}2412 \times 10^{3}$
0·84	$-1{\cdot}8663 \times 10^{-1}$	$-2{\cdot}0675 \times 10^{-2}$	$-5{\cdot}5757 \times 10^{1}$	$9{\cdot}0823 \times 10^{3}$
0·96	$-2{\cdot}0505 \times 10^{-1}$	$-2{\cdot}2748 \times 10^{-2}$	$-5{\cdot}3576 \times 10^{1}$	$9{\cdot}7826 \times 10^{3}$
1·08	$-2{\cdot}1793 \times 10^{-1}$	$-2{\cdot}0540 \times 10^{-2}$	$-4{\cdot}8344 \times 10^{1}$	$1{\cdot}0695 \times 10^{4}$
1·20	$-2{\cdot}2204 \times 10^{-1}$	$-1{\cdot}9191 \times 10^{-2}$	$-4{\cdot}4525 \times 10^{1}$	$1{\cdot}0484 \times 10^{4}$

methods of this report and the finite difference methods of references [19, 20] are in very good agreement.

As a second example, we analyze the cylindrical shell shown in Figure 2 of reference [18] for its symmetric vibration frequencies and maximum deflection under the static loading given therein and compare the results with values reported therein as found by the use of finite elements. Our comparison solutions may be found by analysis of the cylindrical shell

TABLE 4

Example parabolic shell solutions for $w(s, t)$, $u_\phi(s, t)$, at $\theta = 0$ and $t = 1{\cdot}20 \times 10^{-3}$ s by the temporal finite difference method with $\Delta s = 0{\cdot}3220$ in and $\Delta t = 1{\cdot}15 \times 10^{-5}$ s

s(in)	$w(s, t)$(in)	$u_\phi(s, t)$(in)
0·00	0	0
1·93	$-1{\cdot}2055 \times 10^{-2}$	$5{\cdot}3885 \times 10^{-3}$
3·86	$-2{\cdot}7020 \times 10^{-2}$	$9{\cdot}0855 \times 10^{-3}$
5·79	$-4{\cdot}0196 \times 10^{-2}$	$1{\cdot}1132 \times 10^{-2}$
7·72	$-6{\cdot}0249 \times 10^{-2}$	$1{\cdot}1636 \times 10^{-2}$
9·66	$-8{\cdot}4288 \times 10^{-2}$	$1{\cdot}0634 \times 10^{-2}$
11·59	$-1{\cdot}0309 \times 10^{-1}$	$8{\cdot}3639 \times 10^{-3}$
13·52	$-1{\cdot}2015 \times 10^{-1}$	$5{\cdot}1113 \times 10^{-3}$
15·45	$-1{\cdot}3809 \times 10^{-1}$	$1{\cdot}1517 \times 10^{-3}$
17.38	$-1{\cdot}6071 \times 10^{-1}$	$-3{\cdot}3673 \times 10^{-3}$
19·32	$-1{\cdot}8527 \times 10^{-1}$	$-8{\cdot}3433 \times 10^{-3}$
21·25	$-2{\cdot}0548 \times 10^{-1}$	$-1{\cdot}3668 \times 10^{-2}$
23·18	$-2{\cdot}2204 \times 10^{-1}$	$-1{\cdot}9191 \times 10^{-2}$

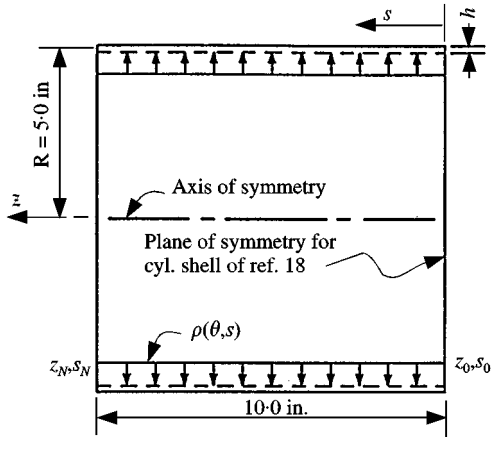

Figure 5. Example cylindrical shell under axisymmetric static loading. The boundary conditions at s_0 are $u_\phi = 0$, $u_\theta = 0$, $\beta_\phi = 0$, and $Q = 0$. The boundary conditions at s_N are $w = 0$, $u_\theta = 0$, $N_\phi = 0$, and $M_\phi = 0$. The thickness $h = 0{\cdot}008$ in. The radial loading $\rho(\theta, s) = 1{\cdot}0$ psi.

and loading shown in Figure 5. For the boundary conditions, we have u_ϕ, u_θ, β_ϕ, and Q equal to zero at s_0 and w, u_θ, N_ϕ, and M_ϕ equal to zero at s_N. The only Fourier component of loading is $p_0 = 1{\cdot}00$ lb/in^2. We take, as in reference [18], a value of $29{\cdot}6 \times 10^6$ lb/in^2 for E, a value of 0·2835 lb/in^3 for γ, and a value of 0·29 for ν. We obtain solutions for finite difference meshes which have 200, 100, and 50 equal increments Δs between node points on the meridional mesh, thus using values of 0·05, 0·10, and 0·20 in, respectively, for Δs. We show in Table 5 the first 21 frequencies as obtained by the finite difference methods of this report for each of the three values used for Δs together with the first 10 frequencies as obtained by the finite element method and reported in reference [18]. It can be seen from Table 5 that the frequencies found by use of finite difference procedures and finite element methods for the example cylindrical shell are in very close agreement but that the finite

TABLE 5

Example cylindrical shell frequencies by finite difference method and reference [18] *finite element method*

Mode no.	Frequencies by F.D.M. (rad/s)			Frequencies by F.E.M. (rad/s)
	$\Delta s = 0{\cdot}05$ in	$\Delta s = 0{\cdot}10$ in	$\Delta s = 0{\cdot}20$ in	
1	$0{\cdot}3000 \times 10^5$	$0{\cdot}3000 \times 10^5$	$0{\cdot}3000 \times 10^5$	$0{\cdot}3001 \times 10^5$
2	$0{\cdot}3981 \times 10^5$	$0{\cdot}3981 \times 10^5$	$0{\cdot}3981 \times 10^5$	$0{\cdot}3983 \times 10^5$
3	$0{\cdot}4005 \times 10^5$	$0{\cdot}4005 \times 10^5$	$0{\cdot}4006 \times 10^5$	—
4	$0{\cdot}4011 \times 10^5$	$0{\cdot}4012 \times 10^5$	$0{\cdot}4014 \times 10^5$	—
5	$0{\cdot}4015 \times 10^5$	$0{\cdot}4015 \times 10^5$	$0{\cdot}4018 \times 10^5$	$0{\cdot}4014 \times 10^5$
6	$0{\cdot}4017 \times 10^5$	$0{\cdot}4018 \times 10^5$	$0{\cdot}4022 \times 10^5$	$0{\cdot}4017 \times 10^5$
7	$0{\cdot}4021 \times 10^5$	$0{\cdot}4022 \times 10^5$	$0{\cdot}4028 \times 10^5$	$0{\cdot}4023 \times 10^5$
8	$0{\cdot}4025 \times 10^5$	$0{\cdot}4027 \times 10^5$	$0{\cdot}4034 \times 10^5$	—
9	$0{\cdot}4031 \times 10^5$	$0{\cdot}4034 \times 10^5$	$0{\cdot}4043 \times 10^5$	$0{\cdot}4032 \times 10^5$
10	$0{\cdot}4040 \times 10^5$	$0{\cdot}4043 \times 10^5$	$0{\cdot}4054 \times 10^5$	—
11	$0{\cdot}4052 \times 10^5$	$0{\cdot}4055 \times 10^5$	$0{\cdot}4067 \times 10^5$	$0{\cdot}4056 \times 10^5$
12	$0{\cdot}4067 \times 10^5$	$0{\cdot}4070 \times 10^5$	$0{\cdot}4084 \times 10^5$	—
13	$0{\cdot}4086 \times 10^5$	$0{\cdot}4090 \times 10^5$	$0{\cdot}4105 \times 10^5$	—
14	$0{\cdot}4111 \times 10^5$	$0{\cdot}4115 \times 10^5$	$0{\cdot}4130 \times 10^5$	$0{\cdot}4113 \times 10^5$
15	$0{\cdot}4142 \times 10^5$	$0{\cdot}4145 \times 10^5$	$0{\cdot}4159 \times 10^5$	—
16	$0{\cdot}4179 \times 10^5$	$0{\cdot}4182 \times 10^5$	$0{\cdot}4193 \times 10^5$	—
17	$0{\cdot}4223 \times 10^5$	$0{\cdot}4225 \times 10^5$	$0{\cdot}4232 \times 10^5$	$0{\cdot}4201 \times 10^5$
18	$0{\cdot}4275 \times 10^5$	$0{\cdot}4276 \times 10^5$	$0{\cdot}4276 \times 10^5$	—
19	$0{\cdot}4337 \times 10^5$	$0{\cdot}4334 \times 10^5$	$0{\cdot}4326 \times 10^5$	—
20	$0{\cdot}4407 \times 10^5$	$0{\cdot}4402 \times 10^5$	$0{\cdot}4381 \times 10^5$	—
21	$0{\cdot}4414 \times 10^5$	$0{\cdot}4414 \times 10^5$	$0{\cdot}4414 \times 10^5$	$0{\cdot}4416 \times 10^5$

element model used in reference [18] does not yield several of the lower frequencies. The maximum radial deflection, $w(s_0)$, is obtained as $0{\cdot}1055743 \times 10^{-3}$ in by use of either of the values of 0·05, 0·10, or 0·20 in for Δs. This compares with a closed form solution value of $0{\cdot}1055743 \times 10^{-3}$ in, which constitutes an exact agreement between the value found by the modal superposition methods of this report and the closed-form solution.

12. CONCLUSIONS

To illustrate the utility of the modal superposition method for shell analysis, we have included dynamic solutions for a parabolic shell as obtained by the modal superposition method and as obtained by the finite difference method used in references [19, 20] for easy comparison. It is seen from a study of the results given in Tables 1–4 that the displacements as found by the modal superposition method (Tables 1 and 2) are in very good agreement with the displacements as found by the temporal finite difference method (Tables 3 and 4). Solutions not shown here for this and other shell examples confirm that as the time increment Δt is reduced the displacements found by the temporal finite difference method will approach the displacements found by the modal superposition method as closely as may be desired (in the absence of significant round-off error). This is true because our finite difference representations for second derivatives of displacements with respect to time approach the true accelerations as Δt approaches zero.

It is seen from the results in Tables 1 and 3 that the values for $N_\phi(s_0, t)$ as found by the modal superposition method are also in very good agreement with the values of $N_\phi(s_0, t)$

given by the temporal finite difference method. Values for $Q(s_0, t)$ are also in reasonably good agreement as found by the two methods. It is not shown herein but at points $s_2 \leqslant s \leqslant s_{N-2}$ for which the finite difference representations for determining the shell influence coefficients and for finding the forces from the nodal displacements are the same, the forces $Q(s, t)$ as found by the modal superposition methods of this report and as found by the temporal finite difference methods of references [19, 20] for this and other shell examples are in very good agreement for all selected times. More accurate values for the shears at and near the boundary edges of the shell may be obtained by suitable reduction of the meridional increment Δs.

To show a comparison with results found by the methods of this report and finite element methods for modal analysis, we have also analyzed the cylindrical shell shown in Figure 2 of reference [18] for its symmetric vibration frequencies and maximum radial deflection for the static loading given therein. Values of the frequencies given in Table 5 show very good agreement of the results found here and in reference [18]. It is seen in Table 5, however, that several of the lower frequencies are not obtained by the finite element mesh used in reference [18] and that a finer finite element mesh would be required to obtain all of the lower and higher frequencies. The finite difference methods of this report are well suited to obtain any desired number of vibration frequencies. For the example cylindrical shell studied here, the maximum deflection found by the modal superposition methods of this report and by closed-form solution are in exact agreement.

The modal analysis methods using finite differences as reported here result in several advantages over other methods described in this report. The use of finite differences is simple to implement and provides solutions for which continuity of all displacements and derivatives thereof exists at every point in the finite difference mesh. The use of multi-segment direct numerical integration as in reference [7] is also avoided. The possible adverse effects of shear locking behavior for finite element formulations for thin shells [27, 32] is also avoided. Use of the modal superposition method itself for analysis also avoids the numerical stability problem associated with explicit numerical step-by-step integration for time-dependent solutions and avoids the need to use a large number of time steps for large values of time t for dynamic solutions.

In summary, we conclude that the modal analysis procedures developed in this report are well suited for determining the linearly elastic shell response of any rotationally symmetric general shell under time-dependent surface loadings (continuous or discontinuous) and due to initial values for the displacements and velocities. Although they are not the most efficient procedures available for obtaining solutions for static loadings, the same procedures may also be used for obtaining such solutions.

REFERENCES

1. R. K. PENNY 1961 *Journal of Mechanical Engineering Science* **3**, 369–377. Symmetric bending of the general shell of revolution by finite difference methods.
2. P. P. RADKOWSKI, R. M. DAVIS and M. R. BOLDUC 1962 *ARS Journal* **32**, 36–41. Numerical analysis of equations of thin shells of revolution.
3. B. BUDIANSKY and P. P. RADKOWSKI 1963 *American Institute of Aeronautics and Astronautics Journal* **1**, 1833–1842. Numerical analysis of unsymmetrical bending of shells of revolution.
4. A. KALNINS 1964 *Transactions ASME* 31*E Journal of Applied Mechanics* **3**, 467–476. Analysis of shells of revolution subjected to symmetrical and nonsymmetrical loads.
5. J. H. PERCY, T. H. H. PIAN, S. KLEIN and D. R. NAVARATNA 1965 *American Institute of Aeronautics and Astronautics Journal* **3**, 2138–2145. Application of matrix displacement method to linear elastic analysis of shells of revolution.

6. A. KALNINS 1964 *Journal of Acoustic Society of America* **36**, 1355–1365. Free vibration of rotationally symmetric shells.
7. H. KRAUS and A. KALNINS 1965 *Journal of Acoustical Society of America* **38**, 994–1002. Transient vibration of thin elastic shells.
8. S. KLEIN 1966 *Shock and Vibration Bulletin* **35**, 27–44. Vibrations of multi-layer shells of revolution under dynamic and impulsive loadings.
9. T. A. SMITH 1970 *U.S. Army Missile Command Technical Report RS-TR*-70-5, *Redstone Arsenal, Alabama*. Numerical solution for the dynamic response of rotationally symmetric shells of revolution under transient loadings.
10. T. A. SMITH 1971 *American Institute of Aeronautics and Astronautics Journal* **9**, 637–643. Numerical analysis of rotationally symmetric shells under transient loadings.
11. T. A. SMITH 1973 *U.S. Army Misile Command Technical Report RL*-73-9, *Redstone Arsenal, Alabama*. Implicit high order finite difference analysis of rotationally symmetric shells.
12. D. BUSHNELL 1973 *Numerical and Computer Methods in Structural Mechanics* 291–336. (S. J. Fenves, N. Perrone and W. C. Schnobrich, editors), New York: Academic Press. Finite-difference energy models versus finite element models: two variational approaches in one computer program.
13. D. BUSHNELL 1977 *Structural Mechanics Software Series*, vol. 1 (N. Perrone and W. Pilkey, editors), 11–143. VA: University Press of Virginia, Charlottesville. BOSOR 4—program for stress, buckling, and vibration of complex shells of revolution.
14. H. RADWAN and J. GENIN JR 1975 *International Journal of Non-Linear Mechanics* **10**, 15–29. Nonlinear modal equations for thin elastic shells.
15. K.-J. BATHE, E. RAMM and E. L. WILSON 1975 *International Journal for Numerical Methods in Engineering* **9**, 353–386. Finite element formulations for large deformation dynamic analysis.
16. T. A. SMITH 1977 *U.S. Army Missile Research and Development Command Technical Report TL*-77-1, *Redstone Arsenal, Alabama*. Explicit high order finite difference analysis of rotationally symmetric shells.
17. T. A. SMITH 1980 *American Institute of Aeronautics and Astronautics Journal* **18**, 309–317. Explicit high-order finite difference analysis of rotationally symmetric shells.
18. Y. B. CHANG, T. Y. YANG and W. SOEDEL 1983 *Journal of Sound and Vibration* **86**, 523–538. Linear dynamic analysis of revolutional shells using finite elements and modal expansion.
19. T. A. SMITH 1983 *U.S. Army Missile Command Technical Report RL*-83-5, *Redstone Arsenal, Alabama*. Finite difference analysis of rotationally symmetric shells under discontinuous distributed loadings.
20. T. A. SMITH 1987 *American Institute of Aeronautics and Astronautics Journal* **25**, 1611–1621. Finite difference analysis of rotationally symmetric shells under discontinuous distributed loadings.
21. S. K. KWOK 1985 *Computers and Structures* **20**, 683–697. Geometrically nonlinear analysis of general thin shells using a curvilinear finite difference (CFD) energy approach.
22. O. S. NARAIKIN 1988 *Soviet Applied Mechanics* **24**, 126–132. Numerical solution method for dynamical problems of shell theory.
23. J. G. TENG and J. M. ROTTER 1989 *Computers and Structures* **31**, 211–233. Elastic–Plastic large deflection analysis of axisymmetric shells.
24. H. WIMMER, 1988 *Acta Mechanica* **73**, 163–175. Application of the two-dimensional Hermitian finite-difference method to linear shear deformation theory of plates and arbitrarily curved shells.
25. T. A. SMITH 1991 *U.S. Army Missile Command Technical Report RD-ST*-91-1, *Redstone Arsenal, Alabama*. Dynamic analysis of rotationally symmetric shells by the modal superposition method.
26. C. H. NORRIS, R. J. HANSEN, M. J. HOLLEY, JR., J. M. BIGGS, S. NAMYET and J. K. MINAMI 1959 *Structural Design for Dynamic Loads*. New York: McGraw-Hill Book Company, Inc.
27. S. S. J. MOY and S. S. E. LAM 1991 *Communications in Applied Numerical Methods* **7**, 377–391. Geometrically non-linear analysis of shell structures.
28. T. A. SMITH 1994 *U.S. Army Missile Command Technical Report RD-ST*-94-12, *Redstone Arsenal, Alabama*. Improved explicit high-order finite difference analysis of rotationally symmetric shells.
29. T. A. SMITH 1995 *U. S. Army Missile Command Technical Report RD-ST*-95-15, *Redstone Arsenal, Alabama*. Finite difference analysis of rotationally symmetric shells using variable node point spacings.
30. T. A. SMITH 1997 *U.S. Army Aviation and Missile Command Technical Report RD-ST*-97-5, *Redstone Arsenal, Alabama*. Improved numerical analysis of rotationally symmetric shells using eight first-order field equations.
31. T. A. SMITH 1998 *U.S. Army Aviation and Missile Command Technical Report RD-PS*-99-1, *Redstone Arsenal, Alabama*. Finite difference analysis of rotationally symmetric shells using variable node point spacings and incorporating matrix stability analysis.

32. H. PARISCH 1995 *International Journal for Numerical Methods in Engineering* **38**, 1855–1883. A continuum-based shell theory for non-linear applications.
33. E. REISSNER 1941 *American Journal of Mathematics* **63**, 177–184. A new derivation of the equations for the deformation of elastic shells.

APPENDIX A: NOMENCLATURE

a_{ij}	elements of matrix A, defined for each Fourier component n by equations (34)
A	coefficient matrix in equation (33) for each Fourier component n, with the eigenvalues removed
$A_1, \ldots, A_9$	coefficients defined in reference [26] for equation (12a)
$B_1, \ldots, B_{12}$	coefficients defined in reference [26] for equation (12b)
$C_1, \ldots, C_8$	coefficients defined in reference [26] for equation (12c)
D	$Eh^3/12(1-v^2)$, flexural rigidity of the shell
$D_1, \ldots, D_{46}$	coefficients defined in reference [26] for equations (13)–(15)
E	Young's modulus
$f(t)$	time functions used to define the time variation of the applied impulsive loadings
g	acceleration constant
h	thickness of the shell
K	$Eh/(1-v^2)$, extensional rigidity of the shell
$M_\theta, M_\phi, M_{\theta\phi}$	moment stress resultants
n	integer, designating the nth Fourier component
N, Q	effective shear resultants
$N_\theta, N_\phi, N_{\theta\phi}$	membrane stress resultants
p, p_θ, p_ϕ	components of the mechanical surface loads
P_n^i	maximum instantaneous dynamic loading at node point i on the shell meridian for the symmetric Fourier component n
Q_θ, Q_ϕ	transverse shear resultants
r	distance of point on the middle surface of the shell from the axis of symmetry
R_θ, R_ϕ	principal radii of curvature of the middle surface of the shell
s	distance from an arbitrary origin along the meridian of the shell in the positive direction of ϕ
Δs	increment of the space variables
s_0	value of the co-ordinate s at the boundary s_0, denoted also as the boundary z_0, of the shell
s_N	value of the co-ordinate s at the boundary s_N, denoted also as the boundary z_N, of the shell
s_i	point on meridional line of the shell at station i
t	independent time variable
Δt	increment of the time variable t, used to obtain solutions by the temporal finite difference method
t_0	initial value of the time variable t
u_θ, u_ϕ, w	components of displacement of the middle surface of the shell
$U_{\theta n}, U_{\phi n}, W_n$	functions of s which represent the normal mode shapes and define the displacements in the co-ordinate directions $u_{\theta n}$, $u_{\phi n}$, and w_n, respectively, for the nth Fourier component during free vibration of the shell
z	distance of point on the middle surface of the shell measured from the origin along the axis of symmetry
z_0	value of the co-ordinate z at the boundary z_0, denoted also as the boundary s_0, of the shell
z_N	value of the co-ordinate z at the boundary z_N, denoted also as the boundary s_N, of the shell
$\beta_\theta, \beta_\phi,$	angles of rotation of the normal to the middle surface of the shell
γ	weight of shell material per unit volume
δ	flexibility matrix for the discretized shell for the Fourier component n
δ_{ij}	displacement at node point i due to a total distributed unit loading for the Fourier component n at node point j

$\Delta_n^{(i,t)}$ nth symmetric Fourier component of displacements at shell meridional station i and at time t due to impulsive loadings

$\Delta_{In}^{(i,t)}$ nth symmetric Fourier component of displacements at shell meridional station i and at time t due to initial displacements and velocities

$\Delta_{Tn}^{(i,t)}$ nth symmetric Fourier component of displacements at shell meridional station i and at time t due to combined impulsive loadings and initial conditions

$\eta_{mn}(t)$ dynamic load factor for the mth mode of the nth symmetric Fourier component of impulsive loading

$\eta_{mn}^I(t)$ time variation of the mth mode displacements for the nth symmetric Fourier component due to initial displacements and velocities

θ, ϕ, ρ co-ordinates of any point of the shell

λ_{mn} eigenvalue of matrix A, equation (34), for the mth vibration mode of the nth Fourier component, defined by equation (35)

v the Poisson ratio

Φ_{mn}^i mode shape ordinate at node point i for the mth vibration mode of the nth symmetric Fourier component

$\bar{\Phi}_{mn}^i$ mode shape ordinate at node point i for the mth vibration mode of the nth symmetric Fourier component when normalized by equation (41)

ψ_{mn} modal participation factor for the mth vibration mode of the nth symmetric Fourier component of impulsive loading, defined by equation (46)

ω_{mn} circular frequency in rad/s associated with the mth vibration mode of the nth symmetric Fourier component, defined by equation (35)